Promoting effect of Co addition on the catalytic partial oxidation of methane at short contact time over a Rh/MgO catalyst

Seiji Naito [a], Hisanori Tanaka [a], Shigeru Kado [a, 1], Toshihiro Miyao [b], Shuichi Naito [b], Kazu Okumura [c], Kimio Kunimori [a], Keiichi Tomishige [a, *]

[a] Institute of Materials Science, University of Tsukuba, 1-1-1 Tennodai, Tsukuba, Ibaraki 305-8573, Japan

[b] Department of Material and Life Chemistry, Kanagawa University, 3-27-1 Rokkakubashi, Kanagawa-ku, Yokohama 221-8686, Japan

[c] Department of Materials Science, Faculty of Engineering, Tottori University, Koyama-cho Minami, Tottori 680-8552, Japan

*** Corresponding author**

Keiichi Tomishige

Tel./Fax: +81-29-853-5030, E-mail: tomi@tulip.sannet.ne.jp

[1] Present Address:

Research & Development Center, CHIYODA Corporation, 3-13 Moriya-cho, Kanagawa-ku, Yokohama, Kanagawa 221-0022, Japan

Abstract

In catalytic partial oxidation of methane under isothermal conditions, a 0.3 wt% Rh/MgO catalyst modified with Co at a molar ratio of Co/Rh = 1 gave higher CH_4 conversion, selectivities to CO and H_2 than than the unmodified 0.3 wt% Rh/MgO. Characterization results using temperature-programmed reduction, extended X-ray absorption fine structure, and transmission electron microscopy indicate alloy formation between Rh and Co. In catalytic partial oxidation of methane without N_2 dilution, the Rh-Co/MgO catalyst with Co/Rh = 1 suppressed the temperature increase near the catalyst bed inlet and yielded a flat temperature profile. This behavior can be interpreted by higher selectivity in the direct partial oxidation route in the presence of gas-phase oxygen and lower activity in steam reforming of methane in the absence of gas-phase oxygen. The higher performance of Rh–Co/MgO (Co/Rh = 1) than Rh/MgO can result from higher methane dissociation ability and higher reduction degree during the partial oxidation of methane.

Key Words:

Catalytic partial oxidation, Methane, Thermography, Hot spot, Rhodium, Cobalt, Alloy

1. Introduction

Production of synthesis gas from natural gas is important for gas-to-liquid processes and methanol synthesis [1, 2]. Steam reforming of methane has been used conventionally in industry [2–5]. Conventional steam reformers are large and expensive because steam reforming of methane is a highly endothermic reaction, as shown below (Eq. (1)); the reactor must be heated from the outside. Much attention has recently been devoted to catalytic partial oxidation of methane (Eq. (2)) as a compact method for synthesis gas production.

$$CH_4 + H_2O \rightarrow CO + 3H_2 \qquad \Delta H^0_{298\,K} = +206\ kJ{\cdot}mol^{-1} \qquad (1)$$

$$CH_4 + 1/2O_2 \rightarrow CO + 2H_2 \qquad \Delta H^0_{298\,K} = -36\ kJ{\cdot}mol^{-1} \qquad (2)$$

It has been reported that high methane conversion and syngas yield were obtained at short and millisecond contact times in the catalytic partial oxidation of methane [6–13]. Various supported metal catalysts have been tested. It has been concluded that Rh is an effective component [7, 8]. However, the reports on bimetallic catalysts containing Rh are so limited [14]. It has been reported that the alloy formation of Pt, Pd and Rh with Ni was effective to the oxidative steam reforming of methane in terms of the catalytic activity and the suppression of hot spot formation [15, 16]. This property is caused by the Ni metal species maintained even in the presence of gas-phase oxygen through the alloy formation between Ni and noble metals. These reports suggest that the alloying between a noble metal and a base metal can be connected to synergetic effects, which enable the substitution of a noble metal with a base metal.

Here, the effect of addition of Co, Ni and Fe was investigated over Rh/MgO. An effective

modification can decrease the usage of Rh, which has high cost and limited availability. In particular, the effect of modifiers on the temperature profiles of the catalyst bed as well as the methane conversion and selectivities for synthesis gas formation were also investigated.

Hot spot formation is a common problem in the conversion of hydrocarbons to synthesis gas using oxygen in catalytic partial oxidation [17–20] and the oxidative reforming of methane [15, 16, 21, 22]. This phenomenon is attributable to the combustion reaction (Eq. (3)) over catalysts near the bed inlet, which can cause catalyst deactivation through sintering of support materials and aggregation of active metal particles.

$$CH_4 + 2O_2 \rightarrow CO_2 + 2H_2O \qquad \Delta H^0_{298\,K} = -803\ kJ{\cdot}mol^{-1} \qquad (3)$$

This article reports that the addition of Co to 0.3 wt% Rh/MgO in a suitable amount enhanced CH_4 conversion and selectivity for syngas formation, which were beyond those of 1.0 wt% Rh/MgO in the partial oxidation of methane at short contact time. At the same time, results show that Rh/MgO modified with an optimum amount of Co was very effective for suppression of hot spot formation. This high performance results from alloy formation between Rh and Co based on the catalyst characterization.

2. Experimental

2.1 Catalyst preparation

Rh/MgO catalysts were prepared by impregnating MgO with an aqueous solution of $RhCl_3{\bullet}3H_2O$ (Soekawa Chemicals). The MgO was obtained by calcining $MgCO_3$ (Wako Pure

Chemical Industries Ltd.) at 1423 K for 3 h; the BET surface area of the MgO was determined to be 6.5 m^2/g. After impregnation, the solvent was evaporated at 353 K and the sample was dried at 383 K for 12 h and then calcined at 773 K for 3 h. Loading amounts of Rh were 0.3–3.2 wt%. Also, Rh/MgO modified with additive metals was also prepared. Co, Ni, and Fe were added by the co-impregnation method using the mixed aqueous solution of $RhCl_3 \cdot 3H_2O$ and corresponding nitrate. After co-impregnation, the solvent was evaporated at 353 K and the sample was dried at 383 K for 12 h and then calcined at 773 K for 3 h. $Co(NO_3)_2 \cdot 6H_2O$, $Ni(NO_3)_2 \cdot 6H_2O$ and $Fe(NO_3)_3 \cdot 9H_2O$ were obtained from Wako Pure Chemical Industries Ltd. Catalysts are denoted as Rh–M/MgO, and the amount of the additives is described by the molar ratio to Rh as in Rh–Co/MgO (Co/Rh = 1). The loading amount of Rh on Rh–M/MgO (M = Co, Ni, Fe) was 0.3 wt%. As a reference, 0.2 wt% Co/MgO was prepared using the impregnation method. A loading amount of 0.2 wt% Co corresponds to a Co amount on Rh–Co/MgO (Co/Rh = 1). In addition, 0.6 wt% Rh–Co/MgO (Co/Rh=1) was also prepared. Catalysts in powder form were pressed and crushed to be sieved into granules of 0.13–0.18 mm. After reduction at 1123 K for 0.5 h, the BET surface area of 0.3 wt% Rh/MgO was determined to be 5.6 m^2/g, and those of Rh–M/MgO (M = Co, Ni, and Fe, M/Rh = 1) were determined respectively to be 5.1, 7.5, and 5.7 m^2/g.

2.2 Catalytic performance in partial oxidation of methane under isothermal conditions

Activity tests for partial oxidation of methane were carried out using a tubular fixed bed flow reactor made of quartz. A thin quartz tube was inserted in the catalyst bed as a thermowell, as illustrated in Figure 1(a). A thermocouple was located at the bottom of the catalyst bed to monitor and

control reaction temperature by furnace heating. The catalyst weight was 10 mg. Catalysts were reduced with hydrogen at 1123 K for 0.5 h before each activity test. To prevent temperature increase of the catalyst bed due to exothermic reactions, the reactant gases ($CH_4 + O_2$) were hugely diluted with N_2 up to $CH_4/O_2/N_2 = 4/2/94$. In fact, no temperature increase was observed at all by infrared thermography. The total flow rate of the gases was 1500 cm^3 min^{-1}, and the contact time was as short as 0.4 ms. Catalytic performance was examined for 0.5 h; steady-state activity and selectivity are shown. The effluent gas was analyzed using an FID-GC equipped with a methanator for CO, CH_4, and CO_2, and a TCD-GC (carrier gas: Ar) for H_2 and a TCD-GC (carrier gas: He) for O_2. Methane conversion and CO and H_2 selectivities are calculated as

CH_4 conversion (%) = $(C_{CO} + C_{CO2})/(C_{CH4} + C_{CO} + C_{CO2})\times 100$,

CO selectivity (%) = $C_{CO}/(C_{CO} + C_{CO2})\times 100$,

H_2 selectivity (%) = $C_{H2}/((C_{CO} + C_{CO2})\times 2)\times 100$,

where C is the concentration of each component in the effluent gases. Throughout all the experiments, no carbon-containing product other than CO and CO_2 was formed. Amount of carbonaceous materials, such as coke deposited on the catalyst surface, was negligible.

2.3 Temperature measurement of catalyst bed with infrared thermography

Reaction tests for partial oxidation of methane ($CH_4/O_2 = 2/1$) without N_2 dilution were carried out using a fixed-bed quartz reactor, as depicted in Figure 1(b) using IR thermography (TH31; NEC San-ei Instruments Ltd.). Since temperature profiles were strongly dependent on catalytic property and performance under the reaction conditions, the profiles were measured using IR thermography, as

reported previously [16, 23]. The catalyst weight was 10 mg and the bed length was 3.0 mm. The furnace temperature was controlled to be 723 K. A cooling trap was located at a reactor exit to remove steam contained in effluent gases. Gas analysis was the same as that used for the activity test in the partial oxidation of methane under isothermal conditions. In experiments for measuring the effect of steam addition to the partial oxidation of methane, steam was obtained by vaporizing distilled water supplied using a feeding pump.

2.4 Characterization of catalysts

Temperature-programmed reduction (TPR) profiles were measured in a fixed-bed quartz reactor. Before TPR measurement, catalysts were treated in O_2 at 773 K for 0.5 h and then in Ar at 773 K for 0.5 h to remove adsorbed species such as CO_2. The sample weight was 50 mg, and the heating rate was 10 K min^{-1} from room temperature to 1123 K, and 5% H_2 diluted in Ar (30 cm^3 min^{-1}) was used. A cold trap with frozen acetone (ca. 173 K) was used for the removal of steam formed. TPR profiles were monitored continuously using an on-line TCD-GC. Consumption of hydrogen was estimated from the integrated peak area of the profiles**.**

Measurement of H_2 chemisorption was carried out in a high-vacuum system using a volumetric method. Before adsorption of H_2, catalysts were treated in H_2 at 1123 K for 0.5 h in a fixed-bed reactor. After this pretreatment, the sample was transferred to a cell for adsorption measurements under air atmosphere. Before each measurement, H_2 pretreatment at 773 K was carried out for 0.5 h in the cell. After evacuation at 773 K, the sample was cooled to room temperature. The total amount of H_2 adsorption was measured at room temperature with a H_2 pressure at adsorption equilibrium of

about 2.6 kPa. The dead volume of the apparatus was 63.5 cm^3 and sample weight was 150 mg.

Transmission electron microscope (TEM) images were taken (JEM-2010F; JEOL) with equipment operated at 200 kV. Catalysts were reduced by H_2 pretreatment at 1123 K for 0.5 h or used for activity tests in the partial oxidation of methane without N_2 dilution for 3.0 h. Samples were dispersed in 2-propanol using supersonic waves. Then they were put on Cu grids for TEM observation under air atmosphere. On the TEM image, small and dark spheres can be assigned to metal particles containing Rh and/or Co. We measured the size of more than 100 particles on several images. The particle sizes were distributed in the range of 1– 11 nm. Average particle size (d) is calculated by $d = \Sigma n_i d_i^3 / \Sigma n_i d_i^2$ (n_i, number of pieces; d_i, particle size) [24].

Rh *K*-edge EXAFS were measured at BL01B1 station in SPring-8 with support from the Japan Synchrotron Radiation Research Institute (JASRI) (Proposal No. 2006A1058). The storage ring was operated at 8 GeV. A Si (311) single crystal was used to obtain a monochromatic X-ray beam. Two ion chambers filled with 50%Ar+50%N_2 and 75%Ar+25%Kr were used, respectively, as detectors of I_0 and I. Co *K*-edge EXAFS was measured at BL-9C station of the Photon Factory at the High Energy Accelerator Research Organization (Proposal No. 2006G095). The storage ring was operated at 2.5 GeV. A Si (111) single crystal was used to obtain a monochromatic X-ray beam. The monochromator at both rings was detuned to 60% maximum intensity to avoid higher harmonics in the X-ray beam. Two ion chambers filled with N_2 and 25%Ar diluted with N_2 for Co *K*-edge EXAFS were used, respectively, as detectors of I_0 and I. Samples for the EXAFS measurement were prepared by pressing catalyst powders of 750 and 250 mg, respectively, for Rh and Co *K*-edge EXAFS. The catalyst

powder was treated using H_2 at 1123 K for 0.5 h in a fixed-bed reactor and the sample was pressed into a self-supporting 7-mm-diameter wafer under atmosphere, followed by treatment of the wafer with H_2 at 773 K for 0.5 h in a cell. After this pretreatment, the sample wafer was transferred to the measurement cell using a glove box filled with nitrogen to prevent exposure of the sample disk to air. The Rh-*K* edge EXAFS data were collected in a transmission mode at room temperature. The Co-*K* edge EXAFS data were collected in a fluorescence mode at room temperature. For the EXAFS analysis, oscillation was first extracted from EXAFS data using a spline smoothing method [25]. The oscillation was normalized by the edge height around 50 eV.

2.5 Titration of adsorbed oxygen during partial oxidation of methane

To examine the reduction degree of catalysts during partial oxidation of methane, titration of adsorbed oxygen with H_2 pulses was carried out after pulse reaction of partial oxidation of methane. The reactor was the same as that depicted in Figure 1(b). Pulses of $CH_4 + O_2$ ($CH_4/O_2 = 2/1$) and H_2 were supplied using six-way valves. The pulse contents were 4.06 μmol CH_4 + 2.03 μmol O_2 and 0.045 μmol H_2. The catalyst amount was 10 mg, where Rh amount was as small as 0.31 μmol. The flow rate of He carrier gas was 300 cm^3 min^{-1}. After H_2 pretreatment, the CH_4/O_2 pulse was introduced 10 times. Reactants and products were analyzed using a quadrupole mass spectrometer (QMS, QMA200; Pfeiffer Vacuum Technology AG). Catalytic performance such as CH_4 conversion, H_2 selectivity, and CO selectivity were based on an average of 10 pulses.

2.6 Methane dissociation ability using a pulse of CH_4+D_2

To evaluate methane dissociation activity, a pulse reaction of $CH_4 + D_2$ was carried out. The

apparatus was the same as that for the CH_4/O_2 reaction. Catalysts were reduced with hydrogen at 1123 K for 0.5 h before the CH_4-D_2 reaction. Pulse gases (CH_4/D_2 = 3.05/3.05 μmol) were introduced to the 10 mg catalyst (Rh: 0.31 μmol) at flow rate of 30 cm^3 min^{-1} of N_2 carrier.

3. Results and discussion

3.1 Catalytic performance in partial oxidation of methane under isothermal conditions

Table 1 shows effect of Rh loading amount on the methane conversion and selectivity over Rh/MgO. The conversion and selectivity increased remarkably with increasing Rh loading in the range of 0.3–1.0 wt%. In contrast, they were almost constant in the range of 1.0–3.2 wt% Rh. This activity in catalytic partial oxidation of methane is rather insensitive to the loading amount; this behavior agreed well with that described in a previous report [8]. It seems that turnover frequency of the partial oxidation of methane decreased with increasing Rh loading amount. The effect of adding second metals over 0.3 wt% Rh/MgO is also listed in Table 1. Addition of Fe had a negative effect on the catalytic performance over Rh/MgO. This tendency can be related to the fact that Rh is the most effective component in catalytic partial oxidation of methane, as reported previously [7, 8]. On the other hand, addition of Ni and Co promoted the partial oxidation of methane. In particular, an interesting point is that the performance on Rh–Co/MgO (Co/Rh = 1) with 0.3 wt% Rh exceeded that of 1.0 wt% Rh/MgO. At the same time, Rh-Co/MgO (Co/Rh = 1) gave higher turnover frequency than the Rh/MgO catalysts. Promoting effect of Co addition was also observed on 0.6 wt% Rh–Co/MgO (Co/Rh=1).

Table 2 lists effect of additive amount of Co over Rh–Co/MgO. Methane conversion and selectivity were improved by addition of Co up to Co/Rh = 1. However, excessive addition of Co in the range of Co/Rh > 1 decreased the catalytic performance gradually with increasing additive amount of Co. An optimum amount of Co addition was determined to be Co/Rh = 1 over 0.3 wt% Rh/MgO from a viewpoint of conversion and TOF. The amount of H_2 adsorption increased with increasing Co amount on Rh-Co/MgO catalysts. The turnover frequency was maximum at Co/Rh = 1. In addition, the results on 0.2 wt% Co/MgO were also listed in Table 2. Based on the low catalytic activity of the Co/MgO, an interaction between Rh and Co can be connected to higher performance of the Rh-Co/MgO catalysts. Furthermore, we also tested the catalytic performance over the Rh–Co/MgO catalyst (Co/Rh=1) after the H_2 reduction at 1123 K for 3 h, and the result was almost the same as that after the reduction for 0.5 h (Table 2), which can be related to no H_2 consumption was observed when the temperature was maintained at 1123 K for 0.5 h in the TPR profiles as mentioned below.

3.2 Characterization of Rh–Co/MgO catalysts

Figure 2 shows profiles of temperature-programmed reduction (TPR) with H_2 of the catalysts; H_2 consumption data are presented in Table 3. Reduction of Rh species on MgO proceeds in a wide temperature range. According to the previous reports, the H_2 consumption below 673 K is assigned to the reduction of Rh_2O_3, and the H_2 consumption above 673 K is assigned to the reduction of $MgRh_2O_4$ [26–28]. The total amount of H_2 consumption on Rh/MgO was close to the stoichiometry of $Rh^{3+} + 3/2H_2 \rightarrow Rh + 3H^+$, as presented in Table 3, which indicates that almost all the Rh species

are present in a metallic state after the TPR experiment. On Co/MgO, the Co species on MgO were reduced at around 900 K [29]. For Rh–Co/MgO, a TPR peak at 500 K grew with increasing Co amount, where the H_2 can be consumed by the reduction of Rh_2O_3 and Co_3O_4 species [30–32]. This behavior indicates that the Co species on Rh–Co/MgO reduced together with the Rh_2O_3 species on MgO; the presence of Rh promotes reduction of Co. In addition, the Rh and Co species interacted strongly with MgO such as $MgRh_2O_4$ can be reduced at higher temperature than 673 K. From the H_2 consumption amount on Rh–Co/MgO (Co/Rh = 1 and 2) considering H_2 consumption on Rh/MgO and MgO, about 70% of Co species was reduced, based on the assumption $Co_3O_4 + 4H_2 \rightarrow 3Co + 4H_2O$ (Table 3). The presence of unreduced Co species indicates stronger interaction between Co and MgO than that between Rh and MgO.

EXAFS technique is very effective to the structural analysis of bimetallic catalysts when the information can be obtained from both edges of the components. Fourier transformation of the k^3-weighted EXAFS oscillation from k space to r space was performed to obtain a radial distribution function. Inversely Fourier filtered data were analyzed using a curve fitting method [33, 34]. The Fourier transform and Fourier filtering ranges are shown for each result. For a curve fitting analysis, the empirical phase shift and amplitude functions for Rh–Rh, Rh–O, Co–Co, and Co–O bonds were extracted, respectively, from data of Rh foil, Rh_2O_3, Co foil, and CoO. Theoretical functions for Rh–Co and Co–Rh bonds were calculated using the FEFF8.2 program [35]. Analyses of EXAFS data were performed using a software program (REX2000, Version 2.3.3; Rigaku Corp.). Error bars for each parameter in the curve fitting procedure were estimated by stepping each parameter, while

optimizing the other parameters, until *R* factor became two times its minimum value [36]. Figure 3 shows Rh *K*-edge EXAFS results of catalysts after H_2 reduction; curve fitting results are presented in Table 4. On the Rh–Co/MgO catalysts, Rh–Co bonds as well as the Rh–Rh bonds were required for obtaining a good curve fitting result. The coordination number (CN) of the Rh–Co bond increased and the CN of the Rh–Rh bond decreased with increasing Co amount. The bond distance of the Rh–Co bond is 0.257–0.263 nm, which is located between Rh–Rh bond (0.268 nm) in Rh metal and Co–Co bond (0.251 nm) in Co metal. A similar bond length was described in a previous report [30]. At the same time, the Rh-Rh bond distance on the Rh–Co/MgO catalysts is 0.262–0.264 nm, which is shorter than that in Rh metal (0.268 nm). The curve fitting results suggest alloy formation of Rh and Co [30-32, 37-39].

Figure 4 shows Co *K*-edge EXAFS results of catalysts after H_2 reduction; curve fitting results are presented in Table 5. For curve fitting of Co/MgO, both Co–Co and Co–O bonds are needed. In addition, the Co–Rh bond was also contributed on Rh–Co/MgO. The presence of the Co–O bond and its CN are supported by the Co-based reduction degree obtained from the TPR in the case of Rh–Co/MgO (Co/Rh = 1 and 2). As a result, EXAFS analysis and TPR results support the Rh-Co alloy formation. As reported previously, Ni was also alloyed with Rh easily [23]. On the other hand, it is expected that Fe is not alloyed with Rh easily, and this is why decreased performance was seen on Rh-Fe/MgO [40, 41].

From the TEM observation, the average particle size of Rh/MgO and Rh–Co/MgO (Co/Rh=1) after reduction is determined to be 5.5±0.3 nm and 7.6±0.3 nm, respectively. In the EXAFS analysis,

the difference in particle size between Rh/MgO and Rh–Co/MgO (Co/Rh = 1) cannot be detected clearly because both sizes are too large to distinguish using EXAFS analysis. Increase of the particle size by Co addition can be associated with Rh–Co alloy formation because number of metallic atoms in a particle increases. In the reduction pretreatment, Rh species are reduced before the reduction of Co, and the reduced Co species are gradually incorporated into the Rh metal particles, which can explain the larger particle size of Rh–Co/MgO. The adsorption amount of H_2 and the metal dispersion on Rh/MgO and Rh–Co/MgO (Co/Rh = 1 and 2) are also presented in Table 1, where the stoichiometry of adsorbed hydrogen to surface metal Rh and Co atoms is assumed to be 1 [42, 43]. Metal dispersion decreased with increasing amount of Co addition; this tendency agrees well with results obtained from TEM observations.

3.3 Catalytic performance in CH_4/O_2 = 2/1 without N_2 dilution

Regarding the partial oxidation of methane without dilution, the catalyst bed temperature is strongly influenced by the catalytic performance. Therefore, bed temperature profiles were measured using IR thermography. Figure 5 shows the thermographical results over Rh–Co/MgO and Rh/MgO, at a fixed contact time. A very high temperature profile was detected near the bed inlet. The order of the highest bed temperature was as follows: Rh–Co/MgO (Co/Rh = 1) < 0.3 wt% Rh/MgO < 1.0 wt% Rh/MgO < Rh–Co/MgO (Co/Rh = 2). According to the previous report [8], H_2 and CO are formed in the presence of gas-phase oxygen by partial oxidation and in the absence of oxygen by steam reforming over the Rh catalyst. A similar interpretation is applicable to the profiles of 0.3 wt% and 1.0 wt% Rh/MgO. In addition, methane combustion as a side reaction in the presence of gas-phase

oxygen also contributed to the temperature increase at the bed inlet. In contrast, the temperature profile on Rh–Co/MgO (Co/Rh = 1) was rather flat. This result indicates that addition of an optimum amount of Co is effective for suppression of hot spot formation over Rh/MgO.

Figure 6 shows the effect of contact time on the highest bed temperature and catalytic performance in the partial oxidation of methane. Here, the contact time was increased by the decrease in flow rate at a constant catalyst amount. Conversion decreased with decreasing contact time, given a constant catalyst temperature. In the present case, CH_4 conversion increased with decreasing contact time, which indicates that the conversion is influenced by temperature increase more strongly than contact time decrease. On the other hand, Rh–Co/MgO (Co/Rh = 1) gave higher methane conversion than Rh/MgO at the same contact time and at lower bed temperature. Table 6 presents a comparison between the results of the activity tests and the equilibrium gas composition calculated on the assumption that the reaction proceeds in an indirect reaction mechanism [18], where methane reforming reactions proceed after methane combustion. In this case, methane conversion is limited by the reaction equilibrium of methane reforming reactions with H_2O and CO_2, and the gas composition at the outlet temperature in the catalyst bed is determined on the basis of the equilibrium. Both Rh–Co/MgO and Rh/MgO catalysts gave higher conversion and selectivity than those at equilibrium based on the bed outlet temperature. In addition, the conversion and selectivity on Rh–Co/MgO was comparable to those at equilibrium based on the observed highest bed temperature. This behavior is explainable by a much smaller contribution of steam reforming on Rh–Co/MgO (Rh/Co = 1) than that on 0.3 wt% Rh/MgO. This behavior is observed in partial oxidation of methane in the presence of

steam more clearly, as described below. In addition, it is characteristic that the Rh–Co/MgO gave higher methane conversion when both highest bed and outlet temperatures were lower than Rh/MgO. It has been reported that higher conversion and selectivities are favored at higher temperature [44], and hot spot formation can promote the partial oxidation of methane through heat transfer over Ni/Yb_2O_3. This can be interpreted by the steam reforming of methane promoted by the heat from the combustion reaction. In contrast, the tendency was opposite in the present case, which is explainable by a much smaller contributions of steam reforming and a much higher contribution of direct partial oxidation as discussed below.

Figure 7 shows the effect of steam addition on temperature profiles of the catalyst bed. For Rh/MgO, the highest bed temperature decreased remarkably with increased partial pressure of steam. This behavior can result from an increasing contribution of steam reforming of methane, which is highly endothermic. Based on the previous reports [45, 46], the kinetics of steam reforming of methane are independent of steam partial pressure. Therefore, we interpret at present that the steam addition increased the amount of the active metallic species through the increase of the H_2 partial pressure because the Rh species are partially oxidized at the inlet of the catalyst bed. In contrast, steam partial pressure did not affect the temperature profiles on Rh–Co/MgO (Co/Rh = 1) significantly. This tendency is also supported by lower catalytic activity in steam reforming over Rh–Co/MgO (Co/Rh = 1) than Rh/MgO, although the details are not shown here. Flat temperature profiles on Rh–Co/MgO (Co/Rh=1) can be affected by two factors simultaneously. One is a higher selectivity for the direct catalytic partial oxidation of methane, which is less exothermic reaction. The

other is a reduction in steam reforming reaction, which is highly endothermic reaction. Both aspects can contribute to the suppression of hot spot formation through Co addition.

3.4 Reduction degree during the reaction and methane dissociation ability

Table 7 lists the results of the CH_4/O_2 pulse reaction and subsequent titration of adsorbed oxygen species. In the CH_4/O_2 pulse reaction, the amount of CH_4 and O_2 feed was much larger than the number of surface metal atoms. The order of methane conversion in the pulse experiment was the same as that of activity tests under continuous flow conditions. Therefore, it is thought that the steady-state catalyst surface is reproduced in the pulse experiment. We measured the amount of adsorbed and absorbed oxygen by the reaction of H_2 ($O(a) + H_2 \rightarrow H_2O$) after the pulse reaction and the total amount of H_2 consumed in the pulses gave the reduction degree of Rh and Co. The reduction degree was calculated on the basis of H_2 consumption amount on catalysts oxidized under 100% O_2 at 873 K for 30 min. The values of reduction degree were rather small and these cannot be explained by the amount of adsorbed oxygen on the metal surface. In particular, the bulk metallic species were also oxidized during the reaction on Rh/MgO and Rh–Co/MgO (Co/Rh=2). A clear relation between the performance in partial oxidation of methane and the reduction degree was observed. The catalysts with lower reduction degree showed lower conversion and selectivity. This tendency indicates that methane can be activated on the metal surface and not on the oxidized surface [47, 48]. An interesting point is the order of the reduction degree during the reaction: Rh–Co/MgO (Co/Rh = 1) > Rh/MgO > Rh–Co/MgO (Co/Rh = 2). As might be apparent, the oxygen affinity of Co was much higher than that of Rh [49]; it is expected that higher oxygen affinity results in a larger amount of adsorbed and

absorbed oxygen during the reaction and lower reduction degree. This expectation is true for the case of Rh–Co/MgO (Co/Rh = 2), and not for the case of Rh–Co/MgO (Co/Rh = 1). The state of Rh and Co species during the CH_4/O_2 pulse reaction is dependent on the reduction rate of the oxidized species and the oxidation rate of the reduced species. The oxidation rate can increase with Co content because of its high oxygen affinity. On the other hand, regarding the reduction rate, when the reducibility agent is H_2, the reduction rate of the Rh/MgO and the Rh–Co/MgO catalysts is expected to be almost the same as shown in the TPR profiles (Figure 2). However, in fact, the reducing agents during the reaction can be methane, H_2 and CO, and the pressure of the reducing agents can also be dependent on the catalytic activity. The Rh and Co species tend to be present as metallic species when the amount of Co added is optimum because high catalytic activity can compensate for the increase of the oxidation rate. In contrast, when too much Co was added, the oxidation rate can exceed the reduction rate remarkably.

Table 8 lists the CH_4–D_2 reaction results at 573 K for evaluation of the methane dissociation ability. The ability order is as follows: Rh–Co/MgO (Co/Rh = 1) > Rh/MgO > Rh–Co/MgO (Co/Rh = 2). Rh–Co/MgO (Co/Rh = 2) showed a rather low ability in spite of the large amount of the H_2 adsorption. The Co metal surface has been shown to have lower methane activation ability than the Rh metal surface from studies on steam reforming of methane [50]. This property can be connected to the low performance in methane dissociation and partial oxidation of methane. In contrast, Rh–Co/MgO (Co/Rh = 1) has higher methane dissociation ability than Rh/MgO, which can be partly related to a larger amount of H_2 adsorption on Rh–Co/MgO (Co/Rh = 1) (Table 3). Based on the

EXAFS results, it is suggested that the surface Co atoms on the Rh–Co alloy particles with a suitable composition can contribute to methane dissociation and partial oxidation of methane, whose performance is comparable to Rh atoms on Rh–Co alloy and Rh metal particles. At present, the promotion mechanism of methane dissociation ability on Rh–Co/MgO (Co/Rh = 1) is not elucidated. Further investigation is necessary.

4. Conclusions

For the partial oxidation of methane with N_2 dilution, Rh–Co/MgO (Co/Rh = 1) exhibited higher activity and selectivities to H_2 and CO than 0.3 wt% and 1.0 wt% Rh/MgO. Characterization using TPR and EXAFS indicates the formation of a Rh–Co alloy on Rh–Co/MgO catalysts, which is also supported by TEM and adsorption measurements.

In the partial oxidation of methane without N_2 dilution, Rh–Co/MgO (Co/Rh = 1) gave much lower catalyst bed temperatures than Rh/MgO. Addition of steam decreased the highest bed temperature remarkably on Rh/MgO. In contrast, the temperature profile was not influenced by steam addition on Rh–Co/MgO (Co/Rh = 1). These results indicate that Rh/MgO catalyzes the partial oxidation and combustion of methane at the bed inlet in the presence of gas-phase oxygen. This can enhance the temperature drastically. In the downstream, the steam reforming of methane is catalyzed in the absence of oxygen. Addition of Co promoted partial oxidation of methane and suppressed methane combustion over Rh–Co/MgO (Co/Rh = 1) in the presence of gas-phase oxygen; these bring the suppression of hot spot formation. The flat bed temperature profiles on Rh–Co/MgO (Co/Rh = 1)

can be simultaneously affected by two factors: one is higher selectivity for the direct partial oxidation of methane, the other is a reduction in steam reforming of methane. Titration of adsorbed oxygen during the reaction revealed that the reduction degree on Rh–Co/MgO (Co/Rh = 1) was higher than that on Rh/MgO, which is associated with higher methane dissociation ability. The results can explain high performance of Rh–Co/MgO (Co/Rh = 1), and the catalytic performance of Rh-Co/MgO can be dependent on the surface composition of the Rh-Co alloy particles.

Acknowledgments

We sincerely thank Japan Oil, Gas and Metals National Corporation (JOGMEC) and Chiyoda Corporation for financial support.

References

[1] J.R. Rostrup-Nielsen, J. Sehested, J.K. Nørskov, Adv. Catal. 47 (2002) 65.

[2] J.R. Rostrup-Nielsen, in: J.R. Anderson, M. Boudart (Eds.), Catalysis Science and Technology, Springer-Verlag, Berlin, 1984, p. 1.

[3] K. Aasberg-Petersen, J.-H. Bak Hansen, T.S. Christensen, I. Dybkjaer, P.S. Christensen, C. Stub Nielsen, S.E.L. Winter Madsen, J.R. Rostrup-Nielsen, Appl. Catal. A 221 (2001) 379.

[4] J.R. Rostrup-Nielsen, Catal. Rev. 46 (2004) 247.

[5] A.P.E. York, T. Xian, M.L.H. Green, J.B. Claridge, Catal. Rev. 49 (2007) 511.

[6] D.A. Hickman, L.D. Schmidt, J. Catal. 138 (1992) 267.

[7] D.A. Hickman, L.D. Schmidt, Science 259 (1993) 343.

[8] R. Horn, K.A. Williams, N.J. Degenstein, A. Bitsch–Larsen, D.Dalle Nogare, S.A. Tupy, L.D. Schmidt, J. Catal. 249 (2007) 380.

[9] R. Horn, N.J. Degenstein, K.A. Williams, L.D. Schmidt, Catal. Lett. 110 (2006) 169.

[10] K.L. Hohn, L.D. Schmidt, Appl. Catal. A 211 (2001) 53.

[11] R. Horn, K.A. Williams, N.J. Degenstein, L.D. Schmidt, J. Catal. 242 (2006) 92.

[12] R. Horn, K.A. Williams, N.J. Degenstein, L.D. Schmidt, Chem. Eng. Sci. 62 (2007) 1298.

[13] C. Elmasides, T. Ioannides, X.E. Verykios, ALChE Journal 46 (2000) 1260.

[14] B. C. Enger, R. Lødeng, A. Holmen, Appl. Catal. A 346 (2008) 1.

[15] B. Li, S. Kado, Y. Mukainakano, T. Miyazawa, T. Miyao, S. Naito, K. Okumura, K. Kunimori, K. Tomishige, J. Catal. 245 (2007) 144.

[16] Y. Mukainakano, B. Li, S. Kado, T. Miyazawa, K. Okumura, T. Miyao, S. Naito, K. Kunimori, K. Tomishige, Appl. Catal. A 318 (2007) 252.

[17] A.M.D. Groote, G.F. Froment, Appl. Catal. A 138 (1996) 245.

[18] D. Dissanayake, M.P. Rosynek, K.C.C. Kharas, J.H. Lunsford, J. Catal. 132 (1991) 117.

[19] I. Tavazzi, A. Beretta, G. Groppi, P. Forzatti, J. Catal. 241 (2006) 1.

[20] L. Basini, K. Aasber-Petersen, A. Guarinoni, M. Ostberg, Catal. Today 64 (2001) 9.

[21] B. Li, K. Maruyama, M. Nurunnabi, K. Kunimori, K. Tomishige, Ind. Eng. Chem. Res. 44 (2005) 485.

[22] B Li, R Watanabe, K Maruyama, M. Nurunnabi, K. Kunimori, K Tomishige, Appl. Catal. A 290 (2005) 36.

[23] B. Li, K. Maruyama, M. Nurunnabi, K. Kunimori, K. Tomishige, Appl. Catal. A 275 (2004) 157.

[24] Y. Chen, K. Tomishige, K. Yokoyama, K. Fujimoto, Appl. Catal. A 165 (1997) 335.

[25] J. W. Cook, D. E. Sayers, J. Appl. Phys. 52 (1981) 5024.

[26] H. Y. Wang, E. Ruckenstein, J. Catal. 186 (1999) 181.

[27] E. Ruckenstein, H.Y. Wang, J. Catal. 190 (2000) 32.

[28] E. Ruckenstein, H.Y. Wang, Appl. Catal. A 198 (2000) 33.

[29] E. Ruckenstein, H.Y. Wang, Appl. Catal. A 204 (2000) 257.

[30] H.F.J. Van't Blik, D.C. Koningsberger, R. Prins, J. Catal. 97 (1986) 210.

[31] H.F.J. Van't Blik, R. Prins, J. Catal. 97 (1986) 188.

[32] J.H.A. Martens, H.F.J. Van't Blik, R. Prins, J. Catal. 97 (1986) 200.

[33] K. Okumura, J. Amano, N. Yasunobu, M. Niwa, J. Phys. Chem. B 104 (2000) 1050.

[34] K. Okumura, S. Matsumoto, N. Nishiaki, M. Niwa, Appl. Catal. B 40 (2003) 151.

[35] A.L. Ankudinov, B. Ravel, J.J. Rehr, S.D. Conradson, Phys. Rev. B 58 (1998) 7565.

[36] K. Tomishige, K. Asakura, Y. Iwasawa, J. Catal. 149 (1994) 70.

[37] H. Kusama, K. Okabe, H. Arakawa, Appl. Catal. A 207 (2001) 85.

[38] M. Ichikawa, J. Catal. 56 (1979) 127.

[39] M. Ichikawa, J. Catal. 59 (1979) 67.

[40] J. W. Niemantsverdriet, A. M. Van der Kraan, W. N. Delgass, J. Catal. 89 (1984) 138.

[41] A. Fukuoka, T. Kimura, N. Kosugi, H. Kuroda, Y. Minai, Y. Sakai, T. Tominaga, M. Ichikawa, J. Catal. 126 (1990) 434.

[42] K. Kunimori, T. Uchijima, M. Yamada, H. Matsumoto, T. Hattori, Y. Murakami, Appl. Catal. 4 (1982) 67.

[43] R.C. Reuel, C.H. Bartholomew, J. Catal. 85 (1984) 63.

[44] D. Dissanayake, M. P. Rosynek, J. H. Lunsford, J. Phys. Chem. 97 (1993) 3644.

[45] J. Wei, E. Iglesia, J. Catal. 225 (2004) 116.

[46] J. Wei, E. Iglesia, Angew. Chem. Int. Ed. 43 (2004) 3685.

[47] T. Sasaki, K. Nakao, K. Tomishige, K. Kunimori, Appl. Catal. A 328 (2007) 140.

[48] T. Sasaki, K. Nakao, K. Tomishige, K. Kunimori, Chem. Commun. (2006) 3821.

[49] T. B. Reed, Free Energy Formation of Binary Compounds. MIT Press, Cambridge, MA, 1971, p. 67.

[50] E. Kikuchi, S. Tanaka, Y. Yamazaki, Y. Morita, Bull. Jpn. Petrol. Inst. 16 (1974) 95.

Captions

Table 1 Results of activity test in partial oxidation of methane with N_2 dilution and H_2 adsorption.

Table 2 Results of activity test in partial oxidation of methane with N_2 dilution and H_2 adsorption.

Table 3 Results of temperature programmed reduction and metal dispersion.

Table 4 Curve fitting results of Rh-*K* edge EXAFS of reduced catalysts.

Table 5 Curve fitting results of Co-*K* edge EXAFS of reduced catalysts.

Table 6 Comparison between the results of the activity tests and the equilibrium calculation.

Table 7 Catalytic performance of pulse CH_4+O_2 reaction and reduction degree after the reaction.

Table 8 CH_4-D_2 exchange reaction over 0.3 wt% Rh/MgO and Rh–Co/MgO (Co/Rh = 1.0 and 2.0).

Fig. 1 Reactor setup. (a) Partial oxidation of methane with N_2 dilution for isothermal conditions, (b) Partial oxidation of methane without N_2 dilution for the IR thermographical observation.

Fig. 2 TPR profiles of 0.3 wt% Rh–Co/MgO catalysts, as well as those of MgO and Co/MgO.

Reduction degree was calculated as the following reactions:

$Rh_2O_3 + 3H_2 \rightarrow 2Rh + 3H_2O$, $Co_3O_4 + 4H_2 \rightarrow 3Co + 4H_2O$.

Fig. 3 Results of Rh *K*-edge EXAFS analysis of catalysts.

(a) k^3-weighted EXAFS oscillations, (b) Fourier transform of k^3-weighted Rh *K*-edge EXAFS, FT range: 30–130 nm^{-1}, (c) Fourier filtered EXAFS data (solid line) and calculated data (dotted line).

Fig. 4 Results of Co *K*-edge EXAFS analysis of catalysts.

(a) k^3-weighted EXAFS oscillations, (b) Fourier transform of k^3-weighted Co *K*-edge EXAFS, FT range: 30–120 nm^{-1}, (c) Fourier filtered EXAFS data (solid line) and calculated data (dotted line).

Fig. 5 Result of thermographical observation during partial oxidation of methane:

(a) an example of a thermographical image on Rh–Co/MgO (Co/Rh = 1); (b) a picture of the catalyst bed; (c) temperature profiles of catalyst bed during the reaction from thermographical observation. Reaction Conditions: CH_4/O_2 = 2/1; total flow rate 300 cm^3 min^{-1}; total pressure 0.1 MPa; catalyst weight 10 mg; contact time 2.0 ms.

Fig. 6 Effect of contact time in partial oxidation of methane without N_2 dilution on the highest bed

temperature and catalytic performance.

(a) 0.3 wt% Rh/MgO, (b) Rh–Co/MgO (Co/Rh = 1).

Reaction Conditions: CH_4/O_2 = 2/1, total flow rate 300–150 cm^3 min^{-1}; total pressure 0.1 MPa; catalyst weight 10 mg; contact time 2.0–4.0 ms.

Fig. 7 Effect of steam addition to the partial oxidation of methane on temperature profiles.

(a) 0.3 wt% Rh/MgO, (b) Rh–Co/MgO (Co/Rh = 1).

Reaction Conditions: $CH_4/O_2/H_2O$ = 200/100/0–50 cm^3 min^{-1}, total flow rate 300–350 cm^3 min^{-1}, H_2O/CH_4 = 0–0.25; total pressure 0.1 MPa; catalyst weight 10 mg; contact time 2.0–1.7 ms.

Table 1 Results of activity test in partial oxidation of methane with N_2 dilution and H_2 adsorption.

Catalyst	H_2 adsorption (μmol g^{-1}-cat.) [a]	Partial oxidation of methane			
		CH_4 conversion (%) [b]	H_2 selectivity (%) [b]	CO selectivity (%) [b]	TOF (s^{-1}) [c]
0.3 wt% Rh/MgO	3.1	59	86	75	388
0.6 wt% Rh/MgO	5.5	67	86	77	248
1 wt% Rh/MgO	8.3	74	90	83	180
2 wt% Rh/MgO	15.9	78	92	88	99
3.2 wt% Rh/MgO	29.5	79	93	89	54
Rh–Co/MgO (Co/Rh = 1)	3.7	76	95	89	420
Rh–Ni/MgO (Ni/Rh = 1)	3.9	71	90	82	369
Rh–Fe/MgO (Fe/Rh = 1)	3.2	60	78	75	382
0.6 wt% Rh–Co/MgO (Co/Rh = 1)	6.3	83	95	90	268

[a] H_2 adsorption at 298 K,

[b] Reaction conditions: $CH_4/O_2/N_2 = 4/2/94$, total flow rate 1500 cm^3 min^{-1}; T_{TC} = 973 K; total pressure 0.1 MPa; catalyst weight 10 mg; contact time 0.4 ms,

[c] Turnover frequency (TOF) in partial oxidation of methane is calculated on the basis of methane conversion rate and the amount of H_2 adsorption at 298 K.

Table 2 Results of activity test in partial oxidation of methane with N_2 dilution and H_2 adsorption.

Catalyst	H_2 adsorption (μmol g^{-1}-cat.) [a]	Partial oxidation of methane			
		CH_4 conversion (%) [b]	H_2 selectivity (%) [b]	CO selectivity (%) [b]	TOF (s^{-1}) [c]
0.3 wt% Rh/MgO	3.1	59	86	75	388
Rh–Co/MgO (Co/Rh = 0.5)	3.3	63	90	78	391
Rh–Co/MgO (Co/Rh = 1)	3.7	76	95	89	420
Rh–Co/MgO (Co/Rh = 1.5)	3.7	71	88	83	391
Rh–Co/MgO (Co/Rh = 2)	4.1	59	79	72	291
Rh–Co/MgO (Co/Rh = 3)	4.1	54	75	71	266
0.2 wt% Co/MgO	—	1	2	30	—

[a] H_2 adsorption at 298 K,

[b] Reaction conditions: $CH_4/O_2/N_2$ = 4/2/94, total flow rate 1500 cm^3 min^{-1}; T_{TC} = 973 K; total pressure 0.1 MPa; catalyst weight 10 mg; contact time 0.4 ms,

[c] Turnover frequency (TOF) in partial oxidation of methane is calculated on the basis of methane

conversion rate and the amount of H_2 adsorption at 298 K.

Table 3 Results of temperature programmed reduction and metal dispersion.

Catalyst	Loading amount (μmol g^{-1}-cat.)		H_2-TPR H_2 consumption (μmol g^{-1}-cat.)	Amount of reduced Co [a] (μmol g^{-1}-cat.)	Dispersion [b] (%)
	Rh	Co			
0.3 wt% Rh/MgO	31	0	52	—	10.1
Rh–Co/MgO (Co/Rh = 1)	31	31	63	23	6.9
Rh–Co/MgO (Co/Rh = 2)	31	62	107	45	5.3

[a] Assuming that all the Rh species are reduced ($Rh^{3+} \rightarrow Rh^0$) and stoichiometry of the Co reduction ($Co_3O_4 + 4H_2 \rightarrow 3Co + 4H_2O$),

[b] Dispersion was calculated as ($2 \times H_2$ adsorption)/(Rh + reduced Co) × 100.

Table 4 Curve fitting results of Rh-*K* edge EXAFS of reduced catalysts.

Catalyst	Shell	CN [a]	R [b] (10^{-1} nm)	σ [c] (10^{-1} nm)	ΔE_0 [d] (eV)	R_f [e] (%)
0.3 wt% Rh/MgO	Rh–Rh	10.6±0.1	2.68±0.01	0.076±0.002	-0.2±0.4	1.0
Rh–Co/MgO	Rh–Rh	7.4±0.2	2.64±0.01	0.080±0.004	-0.9±0.4	0.5
(Co/Rh = 1)	Rh–Co	3.2±0.2	2.63±0.02	0.080±0.002	-2.2±0.6	
Rh–Co/MgO	Rh–Rh	5.7±0.1	2.62±0.01	0.078±0.001	-1.7±0.9	1.0
(Co/Rh = 2)	Rh–Co	4.8±0.1	2.57±0.01	0.083±0.005	-5.5±0.7	
Rh foil	Rh–Rh	12.0	2.68	0.060	0	

[a] Coordination number.

[b] Bond distance.

[c] Debye-Waller factor.

[d] Difference in the origin of photoelectron energy between the reference and the sample.

[e] Residual factor. Fourier filtering range: 0.153–0.273 nm.

Table 5 Curve fitting results of Co-*K* edge EXAFS of reduced catalysts.

Catalyst	Shell	CN [a]	R [b] (10^{-1} nm)	σ [c] (10^{-1} nm)	ΔE_0 [d] (eV)	R_f [e] (%)
0.2 wt% Co/MgO	Co–Co	3.8±0.1	2.50±0.01	0.086±0.016	-5.7±2.1	0.7
	Co–O	2.9±0.3	2.00±0.03	0.093±0.037	-6.6±5.7	
Rh–Co/MgO (Co/Rh = 1)	Co–Co	3.3±0.1	2.56±0.01	0.084±0.005	-9.5±5.3	0.4
	Co–Rh	3.3±0.1	2.62±0.01	0.073±0.010	10.0±0.8	
	Co–O	2.4±0.3	2.09±0.01	0.070±0.009	4.0±0.2	
Rh–Co/MgO (Co/Rh = 2)	Co–Co	3.6±0.2	2.54±0.01	0.076±0.005	-3.9±0.5	0.6
	Co–Rh	2.4±0.1	2.57±0.01	0.081±0.004	4.6±0.6	
	Co–O	2.6±0.3	2.13±0.01	0.075±0.015	8.3±1.3	
CoO	Co–O	6.0	2.13	0.060	0	
Co foil	Co–Co	12.0	2.51	0.060	0	

[a] Coordination number.

[b] Bond distance.

[c] Debye-Waller factor.

[d] Difference in the origin of photoelectron energy between the reference and the sample.

[e] Residual factor. Fourier filtering range: 0.157–0.272 nm.

Table 6 Comparison between the results of the activity tests and the equilibrium calculation.

Catalyst or condition	Temperature (K)		CH_4 conv. (%)	H_2 sel. (%)	CO sel. (%)
	Highest bed	Outlet			
0.3 wt% Rh/MgO [a]	1093±5	899±5	73	86	90
Rh–Co/MgO [a] (Co/Rh = 1)	955±5	885±5	75	87	89

	Temperature (K)	CH_4 conv. (%)	H_2 sel. (%)	CO sel. (%)
Equilibrium [b]	885	56	82	65
	899	62	84	70
	955	75	91	85

[a] Reaction Conditions: CH_4/O_2 = 2/1, total flow rate 300 cm^3 min^{-1}; total pressure 0.1 MPa; catalyst weight 10 mg; contact time 2.0 ms.

[b] Equilibrium gas composition was calculated on the basis that the partial oxidation proceeds in an indirect route (the reforming reactions after the complete combustion of methane).

Table 7 Catalytic performance of pulse CH_4+O_2 reaction and reduction degree after the reaction.

Catalyst	Pulse CH_4+O_2 reaction [a]			Reduction degree (%) [b]
	CH_4 conversion (%)	H_2 selectivity (%)	CO selectivity (%)	
0.3 wt% Rh/MgO	56	62	55	59
Rh–Co/MgO (Co/Rh = 1)	66	78	75	89
Rh–Co/MgO (Co/Rh = 2)	5	9	13	33

[a] Reaction conditions: CH_4/O_2 = 4.06/2.03 μmol (300 cm^3 min^{-1} He carrier); T_{TC} = 873 K; total pressure 0.1 MPa; catalyst weight 10 mg (0.31 μmol-Rh).

[b] Reduction degree was based on H_2 consumption in titration of adsorbed oxygen with H_2 pulses and calculated as (the H_2 consumption after the pulse CH_4+O_2 reaction) / (the H_2 consumption after O_2 oxidation treatment at 873 K) × 100.

Table 8 CH_4-D_2 exchange reaction over 0.3 wt% Rh/MgO and Rh–Co/MgO (Co/Rh = 1.0 and 2.0).

Catalyst	Composition (%) [a]				
	CH_4	CH_3D	CH_2D_2	CHD_3	CD_4
0.3 wt% Rh/MgO	94	0.5	0.6	1.6	3.6
Rh–Co/MgO (Co/Rh = 1)	92	0.4	1.0	2.4	4.3
Rh–Co/MgO (Co/Rh = 2)	97	0.3	0.3	0.5	2.1

[a] Reaction conditions: CH_4/D_2 = 3.05/3.05 μmol (30 cm^3 min^{-1} N_2 carrier); T_{TC} = 573 K; total pressure 0.1 MPa; catalyst weight 10 mg (0.31 μmol-Rh).

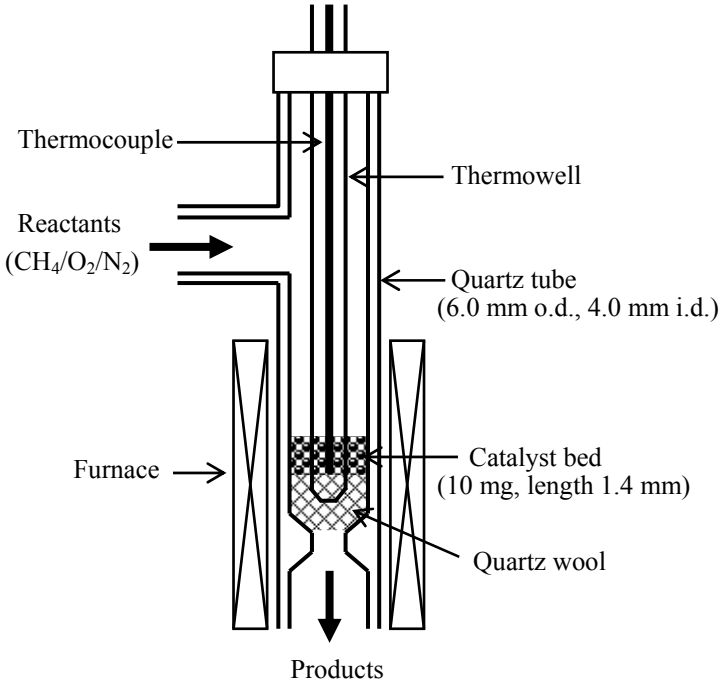

(a)

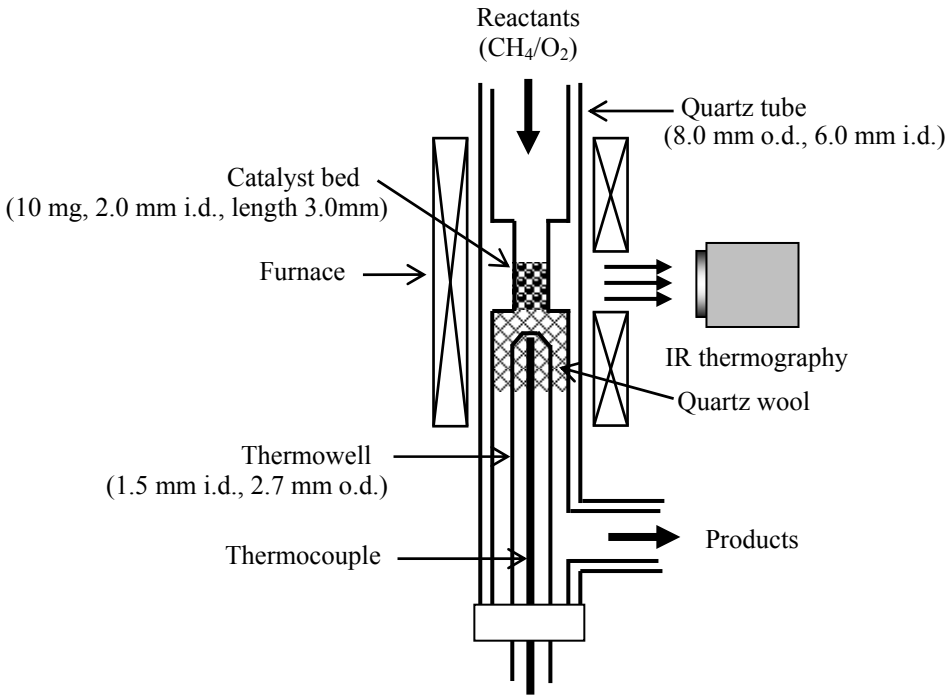

(b)

Fig. 1 Reactor setup. (a) Partial oxidation of methane with N_2 dilution for isothermal conditions, (b) Partial oxidation of methane without N_2 dilution for the IR thermographical observation.

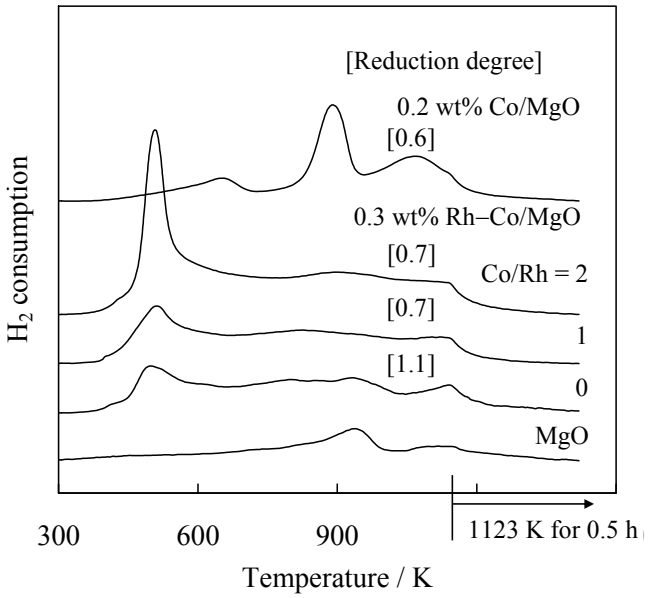

Fig. 2 TPR profiles of 0.3 wt% Rh–Co/MgO catalysts, as well as those of MgO and Co/MgO.

Reduction degree was calculated as the following reactions:

$Rh_2O_3 + 3H_2 \rightarrow 2Rh + 3H_2O$, $Co_3O_4 + 4H_2 \rightarrow 3Co + 4H_2O$.

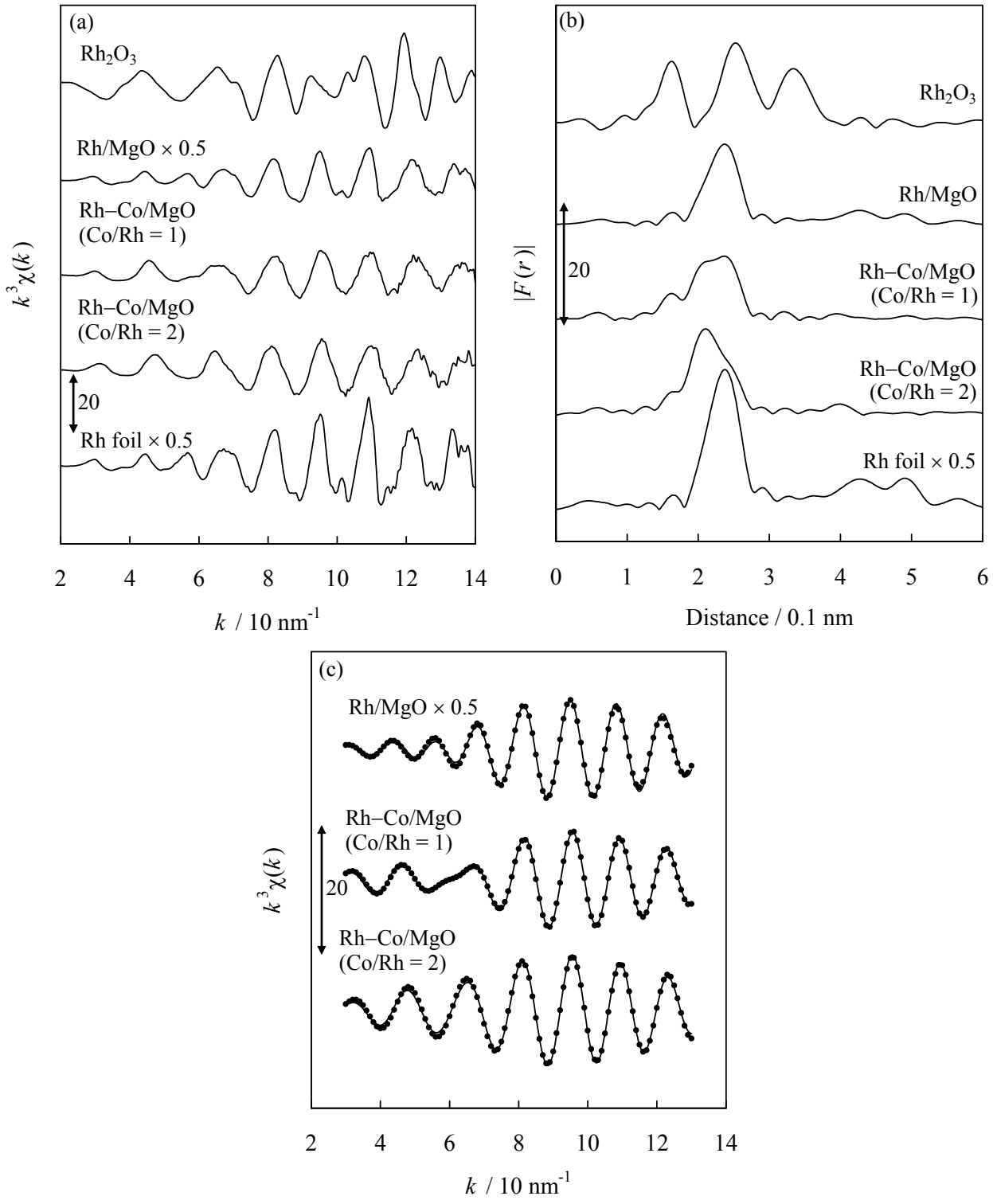

Fig. 3 Results of Rh *K*-edge EXAFS analysis of catalysts.

(a) k^3-weighted EXAFS oscillations, (b) Fourier transform of k^3-weighted Rh *K*-edge EXAFS, FT range: 30–130 nm^{-1}, (c) Fourier filtered EXAFS data (solid line) and calculated data (dotted line).

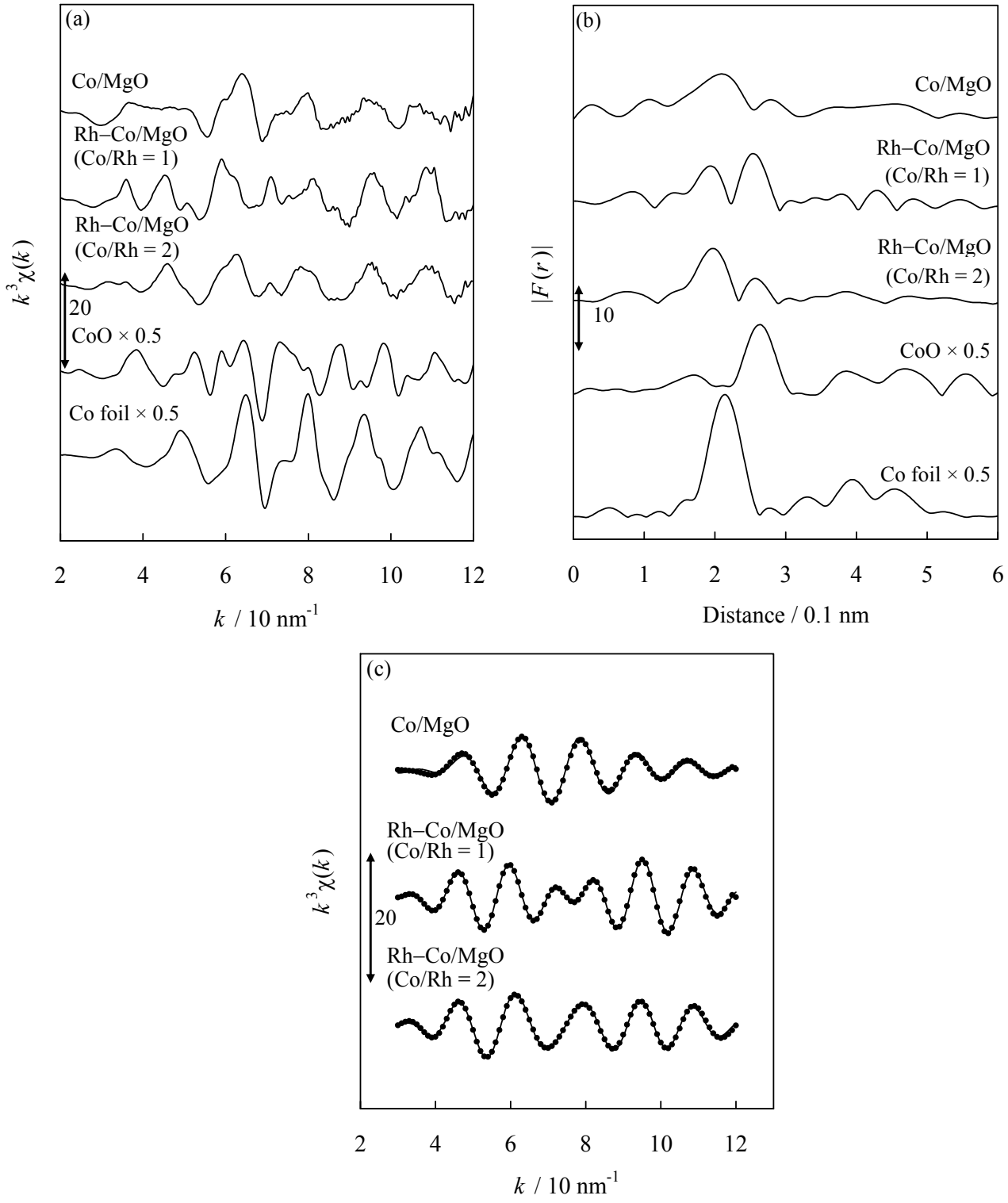

Fig. 4 Results of Co *K*-edge EXAFS analysis of catalysts.

(a) k^3-weighted EXAFS oscillations, (b) Fourier transform of k^3-weighted Co *K*-edge EXAFS, FT range: 30–120 nm^{-1}, (c) Fourier filtered EXAFS data (solid line) and calculated data (dotted line).

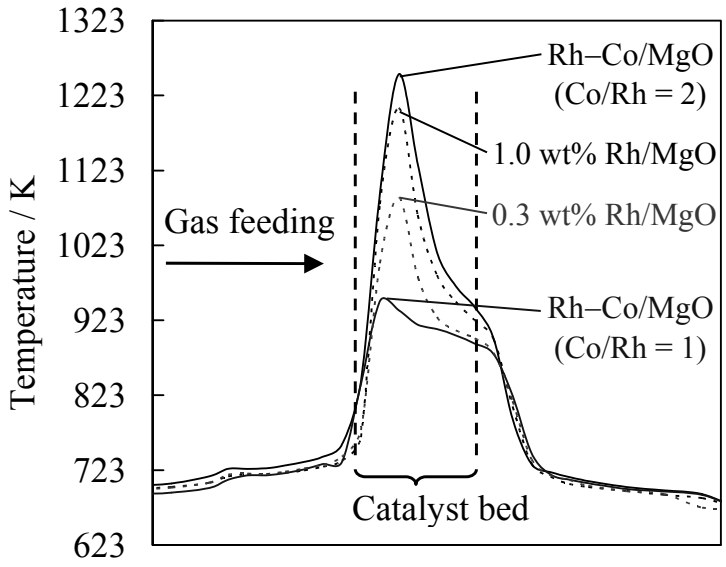

Fig. 5 Result of thermographical observation during partial oxidation of methane: temperature profiles of catalyst bed during the reaction from thermographical observation.

Reaction Conditions: CH_4/O_2 = 2/1; total flow rate 300 cm^3 min^{-1}; total pressure 0.1 MPa; catalyst weight 10 mg; contact time 2.0 ms.

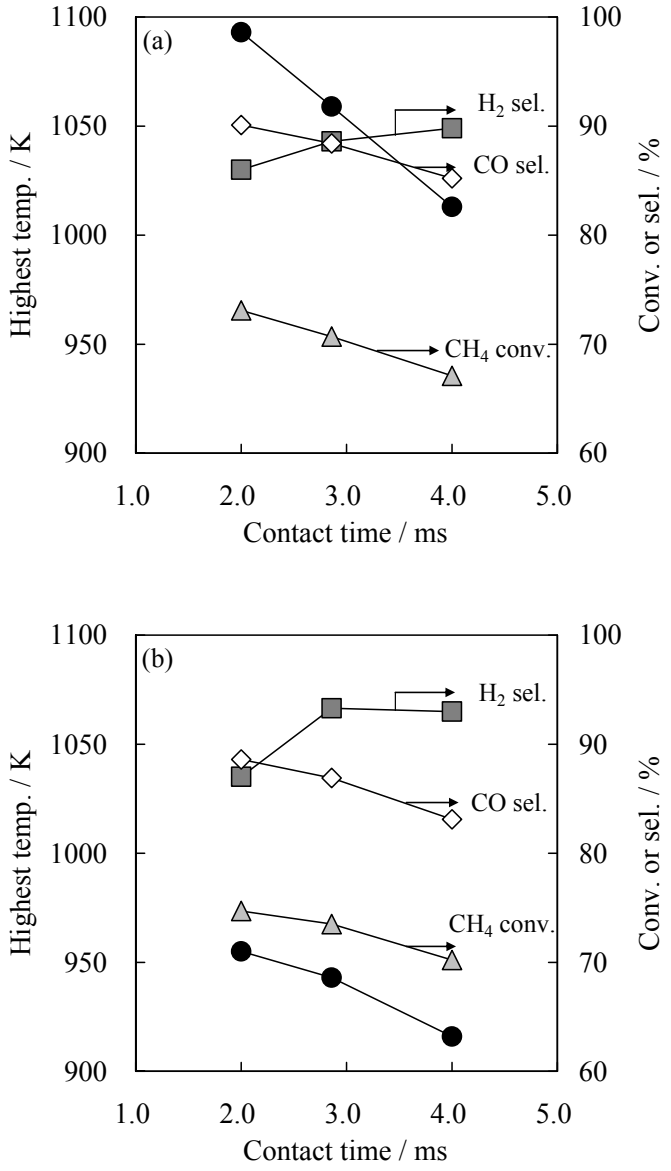

Fig. 6 Effect of contact time in partial oxidation of methane without N_2 dilution on the highest bed temperature and catalytic performance.

(a) 0.3 wt% Rh/MgO, (b) Rh–Co/MgO (Co/Rh = 1).

Reaction Conditions: CH_4/O_2 = 2/1, total flow rate 300–150 cm^3 min^{-1}; total pressure 0.1 MPa; catalyst weight 10 mg; contact time 2.0–4.0 ms.

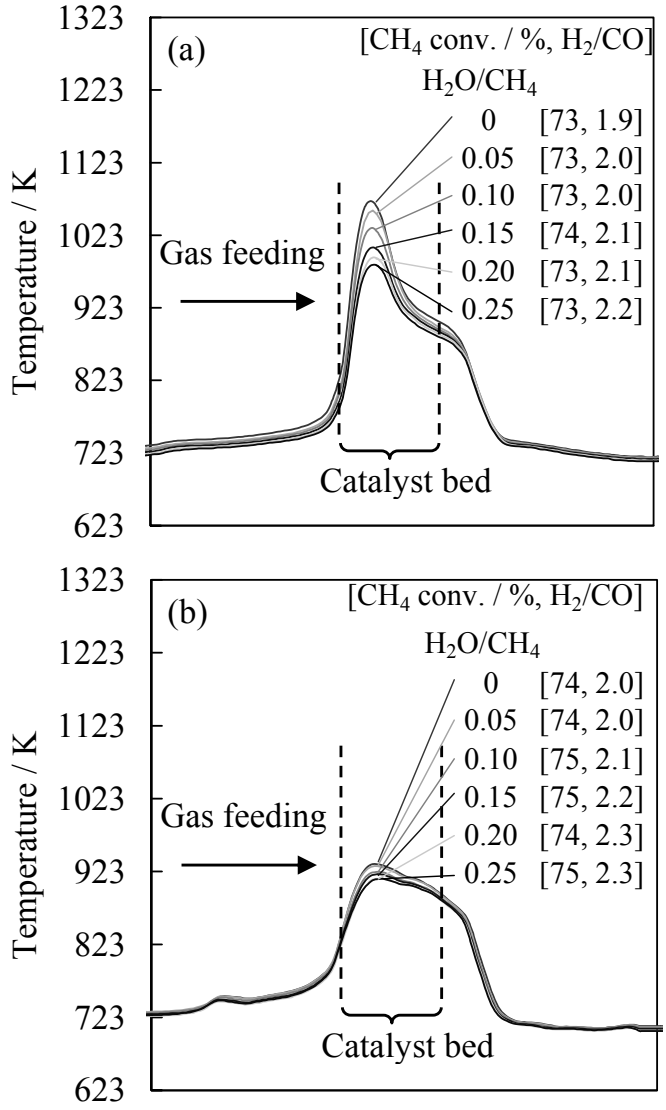

Fig. 7 Effect of steam addition to the partial oxidation of methane on temperature profiles.

(a) 0.3 wt% Rh/MgO, (b) Rh–Co/MgO (Co/Rh = 1).

Reaction Conditions: $CH_4/O_2/H_2O$ = 200/100/0–50 cm^3 min^{-1}, total flow rate 300–350 cm^3 min^{-1}, H_2O/CH_4 = 0–0.25; total pressure 0.1 MPa; catalyst weight 10 mg; contact time 2.0–1.7 ms.